Research Article Vol. 34, No. 2 / 26 Jan 2026 / Optics Express 3222
Optics EXPRESS

Rapid THz nondestructive inspection of medicine capsules

T. H. JEONG,[1] HYEONG-RYEOL PARK,[2] AND Y. H. AHN[1,*]

[1]Department of Physics and Department of Energy Systems Research, Ajou University, Suwon 16499, Republic of Korea
[2]Department of Physics, Ulsan National Institute of Science and Technology (UNIST), Ulsan 44919, Republic of Korea
*ahny@ajou.ac.kr

Abstract: In this study, we developed a screening tool for the rapid identification of defects in two-piece medicine capsules. We used THz time-of-flight (ToF) imaging by incorporating motorized rubber rollers, which allows rapid inspection of the capsules along their cylindrical surface. We obtained 3D images with the cross-sectional information, including the folded area. In particular, THz-ToF images are useful for identifying defects induced by moisture, alien substances, and holes in a nondestructive manner. The statistics for the layer thickness along capsule surfaces enable the rapid quality assessment of capsule quality, while the details on the types of defects can be determined by analyzing the 3D imaging data.

1. Introduction

Terahertz (THz) spectroscopy has significant potential for applications such as material characterization, security screening, telecommunications, sensing, and medical imaging [1–7]. Its ability to penetrate various materials without damage makes it ideal for identifying the underlying structures embedded in non-conductive materials, making them particularly useful in the field of non-destructive testing (NDT). Recent advancements in THz source and detector technologies have enabled the development of highly efficient THz imaging systems for determining the size, shape, and position of conductive objects [8–10]. In addition, THz-NDT imaging is particularly useful for detecting subsurface defects such as cracks or voids in materials such as plastic, ceramic, and composites [11–14]. It is also a valuable tool for quality control and ensuring the integrity of critical components in industries like aerospace and electronics, including integrated circuits [15–17]. Further, the spectral fingerprints provided by THz-NDT imaging could be used to detect illicit drugs and explosives, as well as biomedical purposes [18–21]. As a result of recent advances in compressed sensing algorithms and deep learning–based reconstruction algorithms, image quality and speed have continued to improve [22–25].

In the pharmaceutical industry, stringent standards are required for quality control across all stages, from raw materials and production processes to packaging, labeling, and equipment sterilization [26,27]. Inadequate quality control may lead to serious consequences, such as physical harm from side effects or damage to a company's reputation due to diminished product reliability [28–30]. Particularly in the case of medicine capsules, the degree of capsule seal poses a risk of internal drug degradation, emphasizing the importance of quality control. Currently, high-speed camera-based vision inspection systems and laser technology in the visible and infrared spectrum are employed for capsule quality control. However, these methods are largely confined to surface inspection, and thus face limitations in non-destructively penetrating multilayer structures to detect internal defects [31–33]. The examination of pharmaceuticals by X-ray is challenging due to radiation exposure, which may affect sensitive drug compounds; in addition, it is not responsive to soft materials in general [34]. Optical coherence tomography has been

#577130 https://doi.org/10.1364/OE.577130
Journal © 2026 Received 22 Aug 2025; revised 11 Jan 2026; accepted 13 Jan 2026; published 23 Jan 2026

Optics EXPRESS

used to inspect the pharmaceutical film-coating [35,36]; however, the penetration depth is limited for opaque materials, which is common for gelatin capsule enclosures.

THz imaging technology has emerged as an innovative solution to these limitations. Advancements in THz technology have enabled more precise and non-invasive pharmaceutical compound analysis [37–40]. This includes improved detection of counterfeit drugs and enhanced quality control in manufacturing processes. Additionally, THz imaging can assess the structural integrity of tablets without altering their composition. Conversely, the non-destructive inspection of medicine capsules is rarely investigated. Conventional THz imaging is limited for real-time applications due to long measurement times. Further, it is time-consuming to address the entire cylindrical surface of the capsules, which is essential for in-line quality control. Recently, THz time-of-flight (ToF) systems based on rapid time-delay methods have been developed to address this issue [41–43]; for instance, by using asynchronous optical sampling (ASOPS) techniques with two synchronized fiber lasers. THz-TDS scans are acquired at 100–500 Hz, depending on the difference in repetition rates between the two fiber lasers. This has significantly improved THz-TDS scan acquisition speeds, enabling real-time imaging.

In this study, by utilizing a rapid THz-ToF system, we propose a novel screening methodology for non-destructive defect inspection of medicine capsules with defects such as moisture absorption, punctures, and foreign substances. In the experiments, capsules were rotated 360 degrees on a motor-driven roller, and images corresponding to different defects were acquired using rapid THz-ToF technology. The statistics of capsule thickness distribution provide a useful tool for quantitative quality control.

2. Experimental setup

Figure 1(a) shows a schematic illustration of THz-ToF imaging equipped with rubber rollers for screening two-piece medicine capsules. Commercially available ASOPS imaging systems (TERA-ASOPS, Menlosystems GmbH) provide large time-delay ranges of 10 ns using two independent fiber lasers at $\lambda = 1.56$ µm with a repetition rate of around 100 MHz each [42]. In our experiments, the THz-TDS scan rate was 100 Hz, which is determined by the difference in repetition rate between the two lasers. An emission antenna, a detection antenna, a 50:50 beam splitter, and three off-axis parabolic mirrors (OPMs) were used in the THz-ToF unit. Basically, THz beams are collimated from Tx by an OPM (with a focal length of 50 mm), and the reflected beams are focused on Rx by another OPM with the same focal length. To focus the THz beams on the samples, we used an OPM with a short focal length of 25.4 mm (Thorlabs Inc). In comparison to a 50 mm optical parabolic mirror, we enhanced spatial resolution by twofold, resulting in a resolution of less than 0.5 mm [44].

In this work, we developed an innovative THz imaging system for non-destructive inspection of cylindrical objects, such as medicine capsules. Importantly, we exploited rubberized rollers for rotating the capsules, whereas the THz-ToF unit moves back and forth in the x-direction as shown in Fig. 1(a). This allows us to achieve phase-sensitive THz signals as a function of three-dimensional parameters, namely time delay (T), x-axis, and angle (θ). This scheme is very useful in the commercial application of in-line tablet product inspection. The rotation speed is determined by the number of image pixels. For example, an angular speed of 3°/s is used for a typical pixel configuration of 100 × 90 pixels, resulting in a total measurement time of approximately 2 min (including interline delay). Under our experimental conditions, neither the spatial resolution nor the intensity fluctuations are affected by the rotational speed of the rollers. A drift along the x-axis may occur because the capsule tends to be inclined toward the thinner side; however, this issue can be readily mitigated by slightly tilting the roller axis. Full-surface pharmaceutical imaging has previously been demonstrated using THz imaging systems equipped with six-axis robotic arms (e.g., TPI Imaga 200; TeraView Ltd.), although such approaches inherently require long measurement times. In contrast, the use of rubberized rollers enables a

Optics EXPRESS

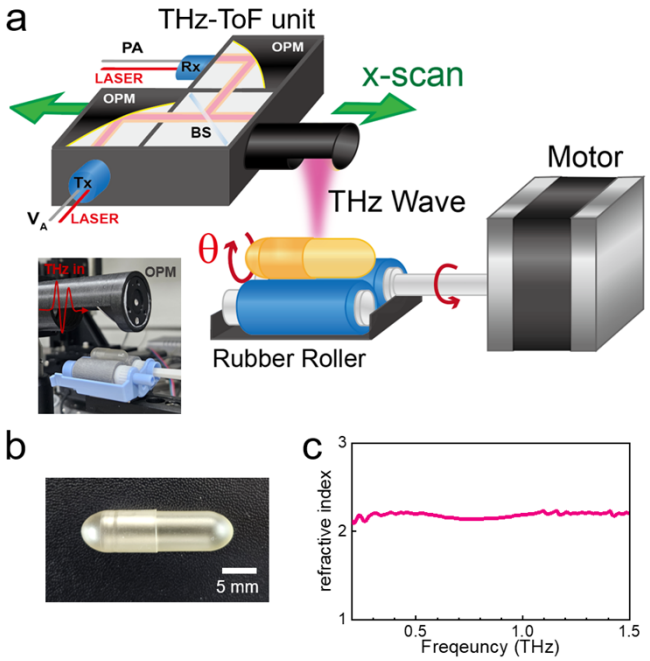

Fig. 1. (a) Schematic illustration of THz time-of-flight imaging setup for inspecting two-piece medicine capsules. The ToF unit is mounted on a translation stage for scanning along the long axis of capsules (x-axis), while the sample is rotated continuously from 0° to 360° by using a rubber roller. OPM: off-axis parabolic mirror, BS: beamsplitter, Tx: THz emitter, Rx: THz receiver, PA: preamplifier. (b) A photograph of a capsule. (c) Refractive index spectrum measured for the capsule with a thickness of 134 µm.

dramatic increase in measurement speed, particularly when combined with THz imaging systems employing high-speed time-delay scanning.

We recorded signals with a delay scan range of $\Delta T = 100$ ps which corresponds to a vertical propagation range of 15 mm in free space. The time delay of THz-ToF signal is equal to depth information, in which 1 ps corresponds to $0.15/n$ mm, where n represents the refractive index of the capsule [41,42]. We determined the refractive index by measuring the transmission of a thin film of capsule with a thickness of 134 µm, which yields 2.1–2.2 (slightly varying with the spectrum). The THz reflection signals were recorded in binary files and analyzed using home-made software. By converting phase-sensitive information into an amplitude envelope, the technique enhances non-destructive imaging results. Using Hilbert transformations, envelope and phase information can be derived from the complex THz signals, $\tilde{E}_{\mathrm{THz}} = \mathrm{Re}(\tilde{E}_{\mathrm{THz}}) + iH[\mathrm{Re}(\tilde{E}_{\mathrm{THz}})]$, where H is the Hilbert transformation [45].

3. Results and discussion

Firstly, we demonstrate THz-ToF results on two-piece capsules without defects. Figure 2(a) illustrates the 2D time-integrated reflection image taken as a function of the position along the long axis of the capsule (x-axis), and another with the rotation angle of the rubberized roller (θ). The scan range was 22 mm × 360° with a pixel size of 110×90 pxl^2. We note that this image has a large pixel size, obtained with a relatively slow scan speed. For non-destructive inspection of capsules, fast imaging at a scan rate of 100 Hz is sufficient in many cases. However, in this particular image, point averaging was applied to present a representative, high-quality image; the

Optics EXPRESS

scan rate was set to 20 Hz (i.e., 20 pixels/s). Shown in Fig. 2(a) is in terms of time-integrated (TI) signals, where the entire depth signal is accumulated at each pixel.

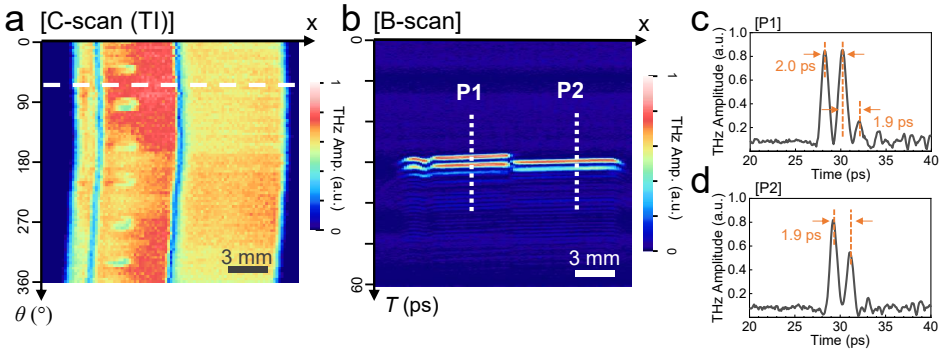

Fig. 2. (a) 2D time-integrated reflection image as a function of the position along the long axis of the capsule (x-axis), and the rotation angle of the rubberized roller (θ). (b) B-scan image as a function of x and the time delay T, along the dashed line in (a). (c),(d) A-scans along the dotted line denoted by P1 (c) and P2 (d).

On the other hand, a B-scan image is shown in Fig. 2(b) along the dashed line in Fig. 2(a), in other words, THz reflection amplitude is plotted as a function of the x-axis and time-delay T. Clearly, we can obtain a cross-sectional image of the two-piece capsules with the top and bottom sides of the thin capsule films. Two layers are visible on the right side, whereas three layers are visible on the left side. This is because the left-hand side is the region in which the two-piece capsules are folded; the bottom layer of the outer piece and the top layer of the inner piece are displayed as a single layer for regular capsules. The 3rd layer at $T = 32$ ps is relatively weak and corresponds to the lower surface of the inner piece. The thickness of the capsule film can be calculated by the time-delay difference of the reflected waves as illustrated by the A-scan plots taken along the P1 (Fig. 2(c)) and P2 (Fig. 2(d)) dotted lines. The time-delay difference between the layers was estimated to be about 1.9 ps which corresponds to 136 μm, considering the refractive index of the film ($n = 2.1$). The statistics of thickness information will be addressed later.

Our THz data can be reconstructed into 3D images as shown in Fig. 3(a). The time-delay range is displayed for $\Delta T = 10$ ps. Here, we plot the THz reflection amplitude at the peak position by fitting the A-scan at each pixel. In particular, we plot the phase-wrapped amplitudes [42]. This means that the positive signal (reddish colors) represents the reflected THz waves without a phase shift, whereas the negative signal (bluish colors) represents the reflected THz waves with a 180-degree phase shift. Clearly, phase shift occurs when the wave is bounced against the air-to-capsule interface (i.e., on the top surface); conversely, no phase shift is observed when it is reflected against the capsule-to-air interface (See the schematic below). Here, ToF-1 illustrates THz amplitudes from the first reflecting surface at each pixel, appearing in blue colors on both the left and right sides. By removing the ToF-1 layer, as shown in Fig. 3(b), one can see the ToF-2 image, which corresponds to the 2nd layer reflection. As expected, no phase shift occurs in the reflected waves on the right-hand side region, which originate from the capsule-air interface. Interestingly, a clear phase shift occurs on the left-hand side for regular two-piece capsules. The outer and inner pieces come into contact in this area with a very narrow air gap in the middle. The air gap is much smaller than the THz pulse temporal pulse-width, hence, it cannot be identified as separate layers. We confirmed this by fabricating an artificial air gap sandwiched between quartz substrates, which showed similar phase-shift characteristics. Accordingly, the reflection

Optics EXPRESS

from the 3rd layer (bottom layer of the inner piece) is shown in the ToF-3 image which illustrates that the positive phase (without the phase shift) is dominant over the surface.

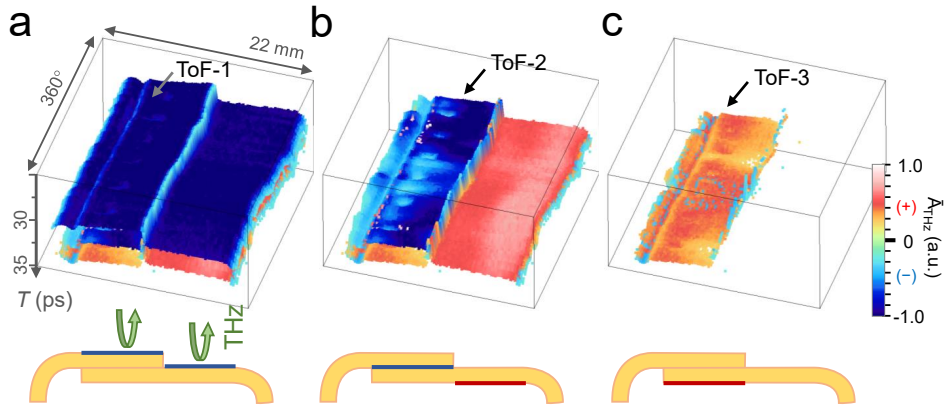

Fig. 3. (a) 3D image of the phase-wrapped amplitude displayed as a function of x, θ, and T. ToF-1 indicates the THz amplitude for the 1st reflection layer of each pixel. (b) 3D image for ToF-2 is shown with the ToF-1 layer removed. (c) 3D image for ToF-3 with ToF-1 and ToF-2 layers removed.

Now we turn to inspection of defective capsules. Distributing defective capsules can have serious health implications for consumers, potentially leading to ineffective treatments or adverse reactions as mentioned above. It also poses significant legal and financial risks for pharmaceutical companies, including costly recalls and damage to their reputations. Therefore, stringent quality control measures are essential to ensure safe and effective products reach the market. A humid environment, in particular, can cause medicines to lose their potency or spoil before their expiration date [46]. This is because pills and capsules are easily damaged by heat and moisture. Figure 4 shows THz-ToF imaging results with a scan range of 20 mm × 360° and a pixel size of 100×90 pxl^2. This is after the capsule is exposed to humid air; in other words, we placed the two-piece capsule in a humid chamber at 80% for 5 minutes before measurements.

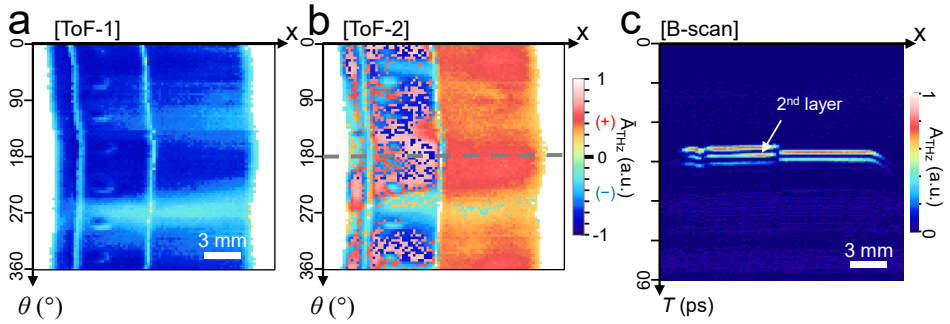

Fig. 4. (a),(b) ToF-1 (a) and ToF-2 (b) images for the defective capsules after exposed to high humidity. The scan range was 20 mm × 360° with a pixel size of 100×90 pxl^2. (c) B-scan image along the dashed line in (b).

We demonstrated a series of ToF-1 (Fig. 4(a)) and ToF-2 (Fig. 4(b)) images in terms of phase-wrapped amplitudes. There are no noticeable changes in the ToF-1 image when compared to the regular capsules in both the left and right regions. Conversely, the ToF-2 image shows dramatic changes in the left region; in other words, the interface between the outer and inner

Optics EXPRESS

pieces has been adversely affected by humidity. There is a large variation in the phase shift of the reflected waves; the red colored region appears in a large portion of the area, unlike in Fig. 3(b). As shown in Fig. 4(c), this is associated with the fact that reflection from the interface (i.e., the 2nd layer) reduces significantly due to the presence of moisture, obscuring the phase information. Alternatively, moisture could induce virtual fusion between the two capsule films, resulting in reduced reflection on the 2nd layer. In this case, the phase of ToF-2 images will be governed by that of the 3rd layer, which is positive. As we will show later, this is consistent with the statistics on film thickness, which exhibit a relatively large portion of the double-layer thickness. Clearly, the inspection of medicine capsules with the ToF-2 image turned out to be a very effective tool for identifying capsules exposed to humid environments.

Other examples of identifying defective capsules are illustrated in Fig. 5. Shown in Fig. 5(a) and 5(b) are the ToF-1 and ToF-2 images, respectively, of the capsules with the alien substance (pharmaceutical powder residue) in the folded area between the outer and inner pieces. The ToF-1 image does not show any indication of defects as in the previous results. Conversely, ToF-2 indicates the marked signature of the defective area, which is painted in red (i.e., the region with the positive phase) on the left-hand side. B-scan image (along the dashed line in Fig. 5(b)) in Fig. 5(c) clearly illustrates that the positive signals are due to the formation of voids in the folded area, which originate from the powder residue in the middle [42].

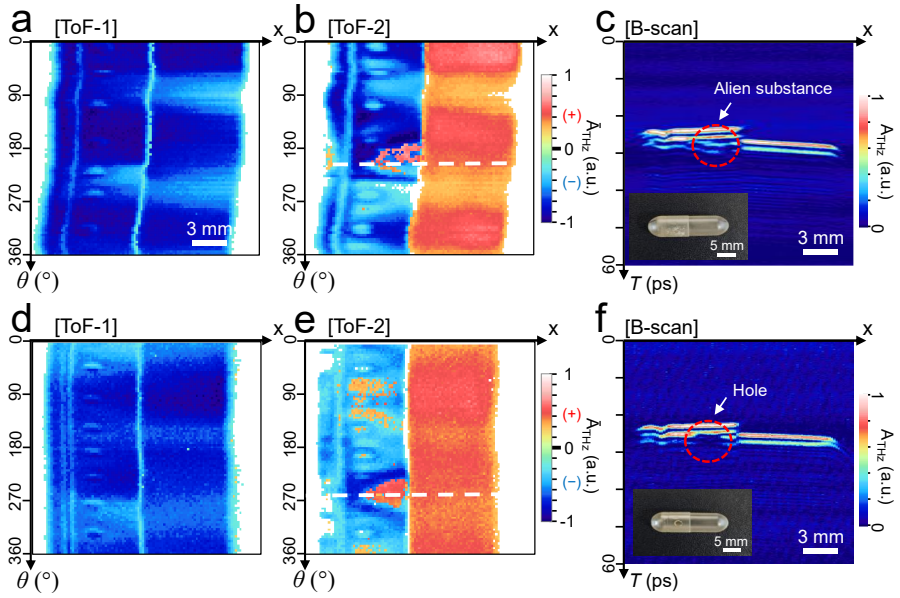

Fig. 5. (a)–(c) ToF-1 (a) and ToF-2 (b) images of the defective capsule with alien substances. The scan range was 20 mm × 360° with a pixel size of 100 × 90 pxl^2. (c) B-scan image along the dashed line in (b). (d)–(f) ToF-1 (d) and ToF-2 (e) images of the defective capsule with a punctured inner piece. The scan range was 20 mm × 360° with a pixel size of 100 × 90 pxl^2. (f) B-scan image along the dashed line in (e).

We also demonstrated THz-ToF imaging on the capsules with a hole in the inner capsule piece, fabricated artificially for a test. A series of ToF-1, ToF-2, and B-scan images (along the dashed line in 5(e)) are shown, respectively, in Fig. 5(d), (e), and (f). Again, the ToF-2 image clearly shows the abnormal region painted in red on the left-hand side. Since the inner piece has a hole structure, the reflected signal from the third layer is missing. The B-scan image along the dashed line illustrates cross-sectional images which confirm the hole structure. Out of the multidimensional data which could be painstaking to analyze, we point out that imaging with

Optics EXPRESS

phase-wrapped ToF-2 (which indicates the second peak of the reflected THz signals) provides the most powerful tool for identifying various defective capsules very rapidly, whereas other approaches such as the B-scan images help to identify the types of the specific defects such as the presence of alien substances and the damages.

Obviously, our imaging technique is powerful for inspecting the thickness of medicine capsules over their cylindrical surface. In Fig. 6, we demonstrate statistics for film thickness obtained for each pixel from the THz-ToF data shown above. We fitted the THz amplitude signal to find the peak positions of each pixel when the amplitudes are above threshold values. The time-delay between the peaks was converted into the thickness (d_{capsule}) from the relation of $d_{\text{capsule}} = 150\Delta T/n$ (μm), where $n = 2.1$ is the refractive index of the film and ΔT is the time-delay difference measured in ps. In Fig. 6(a), we demonstrate a 2D distribution of the film thickness measured between the 1st (ToF-1) and 2nd (ToF-2) layers, with d_{capsule} values ranging from 110 μm to 150 μm. The thickness was found to be relatively higher for the left side, because the presence of the small airgap between the outer and inner capsules can affect the measured values. Finally, we show the histograms for the entire data for the regular capsule and the defective capsules in Fig. 6(b)-(d). We included the film thickness for both the outer and inner pieces including the parts hidden behind the outer piece (by measuring the distance between ToF-2 and ToF-3), which is not shown here.

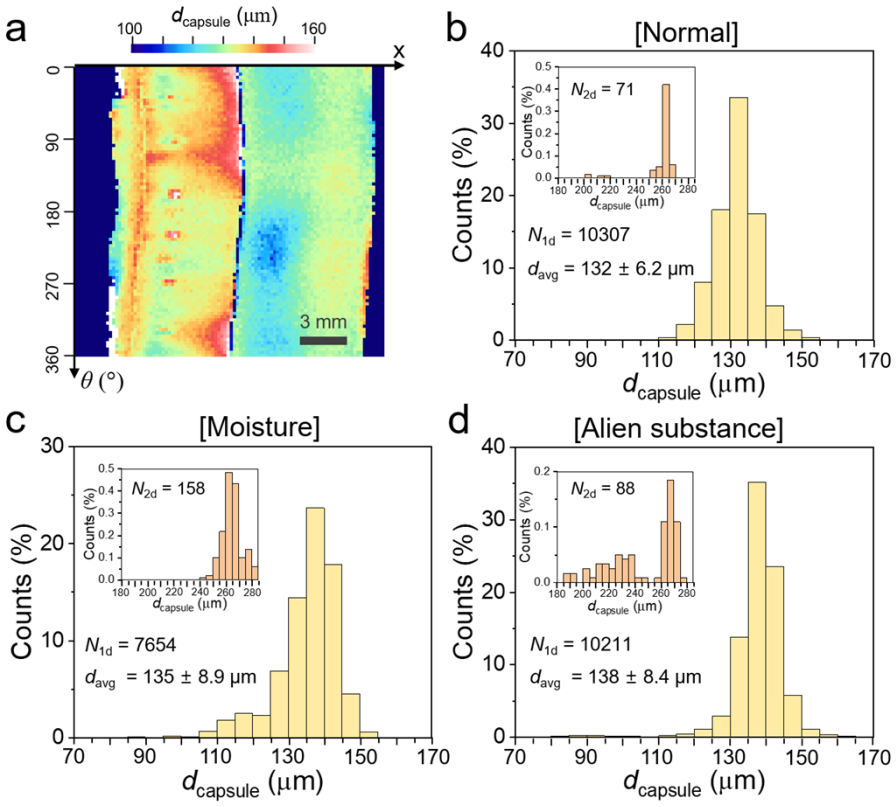

Fig. 6. (a) Capsule thickness distribution (i.e., the distance between the 1st and 2nd layers) for normal sample. (b)–(d) Histogram for film thickness obtained by fitting the peaks in A-scan each pixel for normal sample (b) and defective samples with high moisture-induced damage (c), and alien substances (d). (Insets) Histogram for the data with a double-layer thickness.

Optics EXPRESS

The histogram for the non-defective capsule in Fig. 6(b) demonstrated an average thickness of d_{avg} = 132.0 µm with a standard deviation of σ = 6.2 µm. The number of effective points was N_{1d} = 10307. Shown in the inset is the histogram for double-layer thickness measured at around 260 µm, which corresponds to the pixels with a missing middle layer. Depicted by the white color (>160 µm) in Fig. 6(a) falls into this category. The number of pixels with a double-layer (N_{2d}) occupies only 0.6% of the entire points (i.e., $N_{1d} + N_{2d}$) for the normal sample. By contrast, the histograms for the defective capsules in Fig. 6(c) and (d) show results that deviate from the normal samples in terms of the average values, deviations, and double-layer point occupancy. For instance, for the capsules exposed to high humidity (Fig. 6(c)), we obtained d_{avg} = 135.3 µm and a relatively large standard deviation of σ = 8.9 µm. Besides, the number of single-layer points was lower with N_{1d} = 7654 with a large double-layer occupancy. Histograms for other defective capsules also show relatively broad distribution for the single- and double-layer points, with smaller N_{1d} values in general. Therefore, the statistical approach to the layer thickness provides an efficient tool for the rapid quality inspection of the defective capsules for the products in-line, whereas further analysis on the ToF imaging allows us to identify the types of defects as discussed above.

While previous studies on tablets or capsules were limited to measurements on specific surfaces, full-surface measurements of cylindrical objects have only been implemented at very slow speeds using robotic arms as mentioned above. In contrast, the method proposed in this study—although the measurement time depends on the number of pixels—requires only approximately 2 minutes, representing a dramatic improvement over conventional measurement approaches. When the number of pixels is reduced to a 50×50 grid, the total measurement time can be shortened to within 30 seconds. Nevertheless, the current performance is still insufficient for in-line measurements on production lines, where a large number of capsules must be inspected rapidly. Systems capable of increasing the current per-pixel measurement rate of 100 pixels/s to several kilohertz or higher have already been developed [47], and with the continued advancement of THz-TDS systems, a substantial improvement in measurement speed is expected. This progress will accelerate the commercialization of THz-based non-destructive inspection techniques.

4. Conclusion

In this study, we developed a novel screening tool for the rapid identification of defects in two-piece medicine capsules. We used THz time-of-flight imaging by utilizing high-speed THz TDS systems based on the ASOPS technique. Importantly, we incorporated a motorized rubber roller to rotate the capsule for scanning along its cylindrical surface, while the THz-ToF unit is raster-scanned along the long axis. We obtained cross-sectional images in a non-destructive manner, which allows a rapid inspection of capsules along their cylindrical surfaces, including the inner capsule folded over the outer capsule. THz-ToF images are particularly useful for identifying defects such as moisture-induced damage, foreign substances, and punctured areas. Phase-wrapped amplitude mapping of the respective layers is useful in locating defective areas. Moisture-induced damage, for example, affects both the amplitude and phase of ToF-2 signals (i.e., reflected waves from the 2nd layer) significantly in the folded region. There are also different phase characteristics in the region with alien substances and hole structures. Finally, we obtained a layer thickness distribution for both outer and inner capsules. While defect types can be determined by analyzing cross-sectional imaging data, layer thickness statistics enable rapid quality assessment of capsuled tablets. For instance, defected capsules are characterized by a small number of single-layer thicknesses (with large deviations), together with a relatively large portion of double layer thickness. Consequently, THz-ToF imaging combined with a rubber roller will work as a highly effective tool for rapid quality inspection of numerous pharmaceutical tablets; it will also be extended to the rapid non-destructive testing of various cylindrical objects.

Optics EXPRESS

Funding. Midcareer Researcher Program (RS-2024-00335942); Basic Science Research Program (RS-2021-NR060141); National Research Foundation.

Acknowledgments. This work was supported by the Midcareer Researcher Program (RS-2024-00335942) and the Basic Science Research Program (RS-2021-NR060141) through a National Research Foundation grant funded by the Korea Government.

Disclosures. The authors declare no conflicts of interest.

Data availability. Data underlying the results presented in this paper are not publicly available at this time but may be obtained from the authors upon reasonable request.

References

1. M. Koch, D. M. Mittleman, J. Ornik, *et al.*, "Terahertz time-domain spectroscopy," Nat. Rev. Methods Primers **3**(1), 48 (2023).
2. S. Shen, X. Liu, Y. Shen, *et al.*, "Recent advances in the development of materials for terahertz metamaterial sensing," Adv. Opt. Mater. **10**(1), 2101008 (2022).
3. C.-J. Yang, J. Li, M. Fiebig, *et al.*, "Terahertz control of many-body dynamics in quantum materials," Nat. Rev. Mater. **8**(8), 518–532 (2023).
4. P. A. Banks, E. M. Kleist, and M. T. Ruggiero, "Investigating the function and design of molecular materials through terahertz vibrational spectroscopy," Nat. Rev. Chem. **7**(7), 480–495 (2023).
5. C.-H. Feng and C. Otani, "Terahertz spectroscopy technology as an innovative technique for food: Current state-of-the-art research advances," Crit. Rev. Food Sci. Nutr. **61**(15), 2523–2543 (2021).
6. S. Jun and Y. Ahn, "Terahertz thermal curve analysis for label-free identification of pathogens," Nat. Commun. **13**(1), 3470 (2022).
7. S. W. Jun, J. H. Yim, J.-Y. Park, *et al.*, "Graphene oxides as epsilon-near-zero platforms operating in terahertz frequency range," Laser Photonics Rev. **18**(1), 2300726 (2024).
8. D. M. Mittleman, S. Hunsche, L. Boivin, *et al.*, "T-ray tomography," Opt. Lett. **22**(12), 904–906 (1997).
9. K. H. Jin, Y.-G. Kim, S. H. Cho, *et al.*, "High-speed terahertz reflection three-dimensional imaging for nondestructive evaluation," Opt. Express **20**(23), 25432–25440 (2012).
10. H. S. Kim, J. Kim, and Y. H. Ahn, "Terahertz nondestructive time-of-flight imaging with a large depth range," Curr. Opt. Photonics **6**(6), 619–626 (2022).
11. H. Zhong, J. Xu, X. Xie, *et al.*, "Nondestructive defect identification with terahertz time-of-flight tomography," IEEE Sens. J. **5**(2), 203–208 (2005).
12. I. Amenabar, F. Lopez, and A. Mendikute, "In introductory review to thz non-destructive testing of composite mater," J. Infrared Millim. Terahertz Waves **34**(2), 152–169 (2013).
13. P. Lopato and T. Chady, "Terahertz detection and identification of defects in layered polymer composites and composite coatings," Nondestruct. Test. Eval. **28**(1), 28–43 (2013).
14. S. Fan, T. Li, J. Zhou, *et al.*, "Terahertz non-destructive imaging of cracks and cracking in structures of cement-based materials," AIP Adv. **7**(11), 115202 (2017).
15. A. Chopard, Q. Cassar, J. Bou-Sleiman, *et al.*, "Terahertz waves for contactless control and imaging in aeronautics industry," NDT E Int. **122**, 102473 (2021).
16. S.-H. Park, J.-W. Jang, and H.-S. Kim, "Non-destructive evaluation of the hidden voids in integrated circuit packages using terahertz time-domain spectroscopy," J. Micromech. Microeng. **25**(9), 095007 (2015).
17. K. Ahi, S. Shahbazmohamadi, and N. Asadizanjani, "Quality control and authentication of packaged integrated circuits using enhanced-spatial-resolution terahertz time-domain spectroscopy and imaging," Opt. Lasers Eng. **104**, 274–284 (2018).
18. K. Kawase, Y. Ogawa, Y. Watanabe, *et al.*, "Non-destructive terahertz imaging of illicit drugs using spectral fingerprints," Opt. Express **11**(20), 2549–2554 (2003).
19. Y. Shen, A. Lo, P. Taday, *et al.*, "Detection and identification of explosives using terahertz pulsed spectroscopic imaging," Appl. Phys. Lett. **86**(24), 241116 (2005).
20. M. Schirmer, M. Fujio, M. Minami, *et al.*, "Biomedical applications of a real-time terahertz color scanner," Biomed. Opt. Express **1**(2), 354–366 (2010).
21. T. Ouchi, K. Kajiki, T. Koizumi, *et al.*, "Terahertz imaging system for medical applications and related high efficiency terahertz devices," J. Infrared Millim. Terahertz Waves **35**(1), 118–130 (2014).
22. R. I. Stantchev, X. Yu, T. Blu, *et al.*, "Real-time terahertz imaging with a single-pixel detector," Nat. Commun. **11**(1), 2535 (2020).
23. L. Zanotto, R. Piccoli, J. Dong, *et al.*, "Time-domain terahertz compressive imaging," Opt. Express **28**(3), 3795–3802 (2020).
24. B. Dutta, K. Root, I. Ullmann, *et al.*, "Deep learning for terahertz image denoising in nondestructive historical document analysis," Sci. Rep. **12**(1), 22554 (2022).
25. X. Li, J. Li, Y. Li, *et al.*, "High-throughput terahertz imaging: Progress and challenges," Light: Sci. Appl. **12**(1), 233 (2023).
26. J. Mohammed, V. Sharma, N. Ravindra, *et al.*, "A comprehensive review on quality by design (qbd) in pharmaceuticals," Int. J. Health Adv. Clin. Res. **2**, 55–59 (2024).

Optics EXPRESS

27. J. Woodcock, "The concept of pharmaceutical quality," Am. Pharm. Rev. **7**, 10–15 (2004).
28. A. Miglani, C. Saini, P. Musyuni, *et al.*, "A review and analysis of product recall for pharmaceutical drug product," J. Generic Med. **18**(2), 72–81 (2022).
29. J. M. Caudron, N. Ford, M. Henkens, *et al.*, "Substandard medicines in resource-poor settings: A problem that can no longer be ignored," Trop. Med. Int. Health **13**(8), 1062–1072 (2008).
30. Q. Bassat, M. Tanner, P. J. Guerin, *et al.*, "Combating poor-quality anti-malarial medicines: A call to action," Malar. J. **15**(1), 302–312 (2016).
31. N. Prajwala, "Defect detection in pharma pills using image processing," Int. J. Eng. Technol. **7**, 102–106 (2018).
32. R. A. Lodder, M. Selby, and G. M. Hieftje, "Detection of capsule tampering by near-infrared reflectance analysis," Anal. Chem. **59**(15), 1921–1930 (1987).
33. O. Awotunde, J. Lu, J. Cai, *et al.*, "Mitigating the impact of gelatin capsule variability on detection of substandard and falsified pharmaceuticals with near-ir spectroscopy," Anal. Methods **16**(11), 1611–1622 (2024).
34. R. Hanke, T. Fuchs, and N. Uhlmann, "X-ray based methods for non-destructive testing and material characterization," Nucl. Instrum. Methods Phys. Res. A **591**(1), 14–18 (2008).
35. M. Wolfgang, A. Kern, S. Deng, *et al.*, "Ultra-high-resolution optical coherence tomography for the investigation of thin multilayered pharmaceutical coatings," Int. J. Pharm. **643**, 123096 (2023).
36. J. M. A. Mauritz, R. S. Morrisby, R. S. Hutton, *et al.*, "Imaging pharmaceutical tablets with optical coherence tomography," J. Pharm. Sci. **99**(1), 385–391 (2010).
37. A. J. Fitzgerald, B. E. Cole, and P. F. Taday, "Nondestructive analysis of tablet coating thicknesses using terahertz pulsed imaging," J. Pharm. Sci. **94**(1), 177–183 (2005).
38. J.-Y. Kim, H.-J. Song, M. Yaita, *et al.*, "Cw-thz vector spectroscopy and imaging system based on 1.55-μm fiber-optics," Opt. Express **22**(2), 1735–1741 (2014).
39. S. Zhong, Y.-C. Shen, L. Ho, *et al.*, "Non-destructive quantification of pharmaceutical tablet coatings using terahertz pulsed imaging and optical coherence tomography," Opt. Lasers Eng. **49**(3), 361–365 (2011).
40. M. R. Patil, S. B. Ganorkar, A. S. Patil, *et al.*, "Terahertz spectroscopy: Encoding the discovery, instrumentation, and applications toward pharmaceutical prospectives," Crit. Rev. Anal. Chem. **52**(2), 343–355 (2022).
41. J. H. Yim, S.-y. Kim, Y. Kim, *et al.*, "Rapid 3d-imaging of semiconductor chips using thz time-of-flight technique," Appl. Sci. **11**(11), 4770 (2021).
42. H. Yoo, J. Kim, and Y. H. Ahn, "High-speed thz time-of-flight imaging with reflective optics," Sensors **23**(2), 873 (2023).
43. J. Takayanagi, H. Jinno, S. Ichino, *et al.*, "High-resolution time-of-flight terahertz tomography using a femtosecond fiber laser," Opt. Express **17**(9), 7533–7539 (2009).
44. H. Yoo, B. H. Son, J. Kim, *et al.*, "Thz time-of-flight imaging with real-time surface-tracking for enhanced spatial resolution," J. Phys. D: Appl. Phys. **58**(45), 455102 (2025).
45. D.-Y. Kong, X.-J. Wu, B. Wang, *et al.*, "High resolution continuous wave terahertz spectroscopy on solid-state samples with coherent detection," Opt. Express **26**(14), 17964–17976 (2018).
46. A. N. Zaid, "A comprehensive review on pharmaceutical film coating: Past, present, and future," Drug Des Devel Ther. **14**, 4613–4623 (2020).
47. N. Pałka, M. Maciejewski, K. Kamiński, *et al.*, "Fast thz-tds reflection imaging with ecops—point-by-point versus line-by-line scanning," Sensors **22**(22), 8813 (2022).